Altermagnetic Proximity Effect

Ziye Zhu,[1] Richang Huang,[1] Xianzhang Chen,[1] Xunkai Duan,[1] Jiayong Zhang,[1,2] Igor Žutić,[3] and Tong Zhou[1,*]

[1]*Eastern Institute for Advanced Study, Eastern Institute of Technology, Ningbo, Zhejiang 315200, China*
[2]*School of Physical Science and Technology, Suzhou University of Science and Technology, Suzhou, 215009, China*
[3]*Department of Physics, University at Buffalo, State University of New York, Buffalo, New York 14260, USA*

(Dated: September 9, 2025)

Proximity effects not only complement the conventional methods of designing materials, but also enable realizing properties that are not present in any constituent region of the considered heterostructure. Here we reveal an unexplored altermagnetic proximity effect (AMPE), distinct from its ferromagnetic and antiferromagnetic counterparts. Using first-principles and model analyses of van der Waals heterostructures based on the prototypical altermagnet V_2Se_2O, we show that its hallmark momentum-alternating spin splitting can be directly imprinted onto adjacent nonmagnetic layers—a process we term altermagnetization. This is demonstrated in a monolayer PbO through characteristic band splitting and real-space spin densities, with systematic dependence on interlayer spacing and magnetic configuration. We further predict broader AMPE manifestations: Valley-selective spin splitting in a monolayer PbS and a topological superconducting phase in monolayer $NbSe_2$, both inheriting the alternating k-space spin texture of the altermagnet. These results establish AMPE not only as a distinct proximity mechanism, but also as a powerful method of using altermagnetism in designing emergent phenomena and versatile applications.

Proximity effects allow a material to acquire properties of its neighbors, becoming magnetic, superconducting, topologically nontrivial, or exhibiting enhanced spin–orbit coupling [1–3]. Magnetic proximity effects, particularly in ferromagnets, are widely used to generate spin splitting and tune magnetic parameters including anisotropy, coercivity, and exchange bias [3–11]. Antiferromagnetic proximity, in turn, relies on interfacial hybridization without fringing fields, enabling ultrafast spin dynamics and symmetry-enforced transport [1, 12, 13]. These mechanisms underpin modern spintronics, valleytronics, topological states, and heterostructures of superconductors and magnets [14–18].

A growing class of unconventional magnets [19–26], often termed altermagnets (AM) [27–36], exhibits properties beyond common ferromagnets and antiferromagnets, most notably momentum-dependent alternating spin splitting without net magnetization. This nonrelativistic spin splitting and its tunability expand the opportunities in spintronics [37–40], multiferroics [41–47], topology [48–52], and superconductivity [53–57]. A central challenge now lies in understanding if this distinctive magnetic order, rooted in antiferromagnetic (AFM) sublattices linked by symmetries involving rotations [27–30] can be transferred across an interface into otherwise nonmagnetic (NM) layers. Establishing whether AM generate a distinct proximity effect, rather than simply mimicking ferromagnetic or antiferromagnetic proximity, is key to assessing their impact. Equally important is clarifying if this proximity channel can enable unexplored phenomena, particularly in van der Waals (vdW) heterostructures, where proximity effects are most tunable [58–62].

In this work, we address these questions by establishing the concept of the altermagnetic proximity effect (AMPE) as in Fig. 1, whereby the alternating spin splitting intrinsic to AM is transferred across an interface and imprinted on the neighboring nonmagnetic layers. Using first-principles calculations combined with model analysis, we demonstrate how the prototypical AM V_2Se_2O projects its momentum-space spin texture into adjacent materials through an interfacial process we term altermagnetization. We first identify altermagnetic band splitting and real-space spin densities in an altermagnetized monolayer PbO and track their systematic evolution with interlayer spacing and magnetic configuration, establishing the robustness and tunability of AMPE. Beyond this prototypical example, we show that the same mechanism, AMPE, generates valley-dependent spin splitting in a semiconductor PbS and induces a topological superconductivity in the s-wave superconductor $NbSe_2$ [63, 64]. Together, these results establish AMPE as a fundamentally distinct proximity mechanism and a powerful platform for designing multifunctional quantum states in vdW heterostructures.

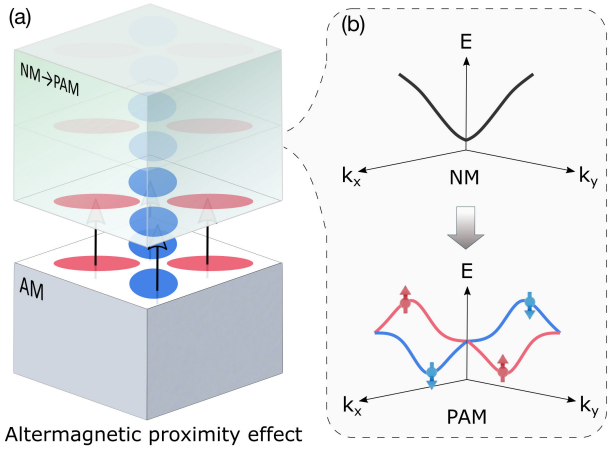

FIG. 1. Schematic of the AMPE. **(a)** AM order penetrating an NM layer. **(b)** Band evolution of the NM layer as it becomes a proximitized altermagnet (PAM).

Our proposed AMPE is schematically illustrated in Fig. 1(a). When an NM material is placed in contact with an altermagnet, the extension of electronic wave functions across

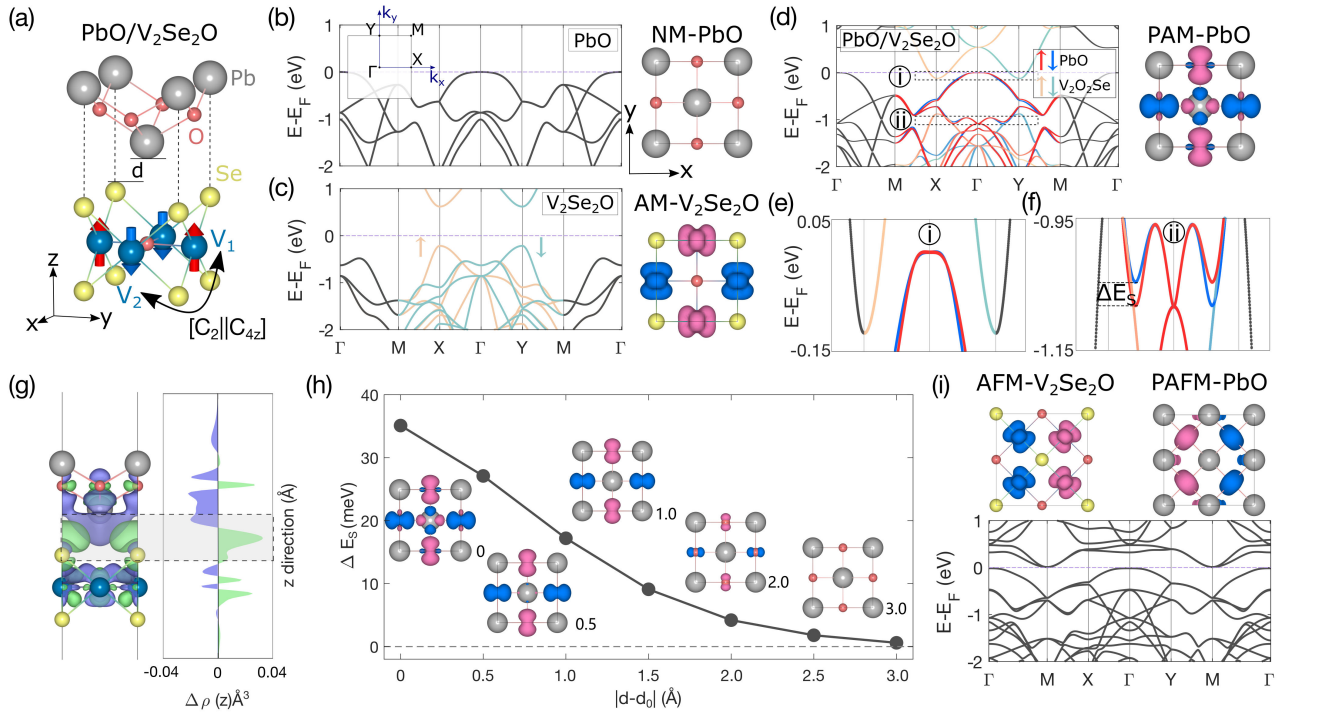

FIG. 2. **(a)** Crystal structure of PbO/V_2Se_2O heterostructure. The spin sublattices of V_2Se_2O are connected by $[C_2\|C_{4z}]$ symmetry. **(b)-(d)** Calculated bands and spin densities of pristine monolayers PbO and V_2Se_2O, and their heterostructure. The inset in **(b)** shows the first Brillouin zone. **(e)** and **(f)** Enlarged views of the regions labeled i and ii in **(d)**. **(g)** Differential charge density of the PbO/V_2Se_2O heterostructure and its planar average, $\Delta q(z)$. Green (purple) indicates charge accumulation (depletion) and the isosurface value is 5×10^{-4} e/bohr^3. **(h)** Spin splitting ΔE_S in **(f)** with the spin densities, as a function of the interlayer distance d in **(a)**, where d_0 is the equilibrium value. **(i)** Same as **(d)** but for a proximitized AFM PbO (PAFM-PbO), realized when PbO is placed on a $\sqrt{2} \times \sqrt{2}$ V_2Se_2O supercell in a conventional AFM state. For all bands, black denotes spin-degenerate states; red and blue indicate spin-up and spin-down bands of the PAM component (PbO), while yellow and green represent the corresponding bands of the V_2Se_2O component.

the interface can imprint the characteristic alternating spin splitting of the AM onto the NM layer. This interfacial process drives a transition from the NM state to a proximitized altermagnet (PAM), in which originally spin-degenerate bands acquire momentum-dependent spin polarization [Fig. 1(b)]. As with other proximity effects [1], AMPE is short ranged and decays with distance from the interface. Two-dimensional vdW systems, with atomically thin layers and clean interfaces, thus provide an ideal platform to exploit this AMPE and to design the corresponding highly tunable functionalities.

While most experimentally confirmed altermagnets exist as bulk crystals or thin films [31–34], V_2Se_2O stands out as a famous vdW candidate [24, 65]. Its intercalated metallic derivatives have also been experimentally identified as altermagnets [33, 34], further highlighting its versatility. V_2Se_2O crystallizes in a square lattice where the two V sublattices form a checkerboard AFM configuration linked by C_{4z} symmetry [Fig. 2(a)]. This symmetry yields the hallmark AM features, as confirmed by our calculations showing alternating spin densities in real space and momentum-dependent spin splitting [Fig. 2(c)]. To demonstrate the AMPE of V_2Se_2O, we select PbO as the adjacent NM layer. PbO is a well-established semiconductor with a simple, well-characterized crystal structure and spin-degenerate bands [66, 67], as shown in our calculations [Fig. 2(b)]. Importantly, PbO and V_2Se_2O both form 2D square lattices with a minimal lattice mismatch of just 0.7%, making PbO an ideal and clean reference to isolate and analyze the AMPE from V_2Se_2O.

To investigate the emergence of AMPE, we computed the total energies of several stacking configurations of the PbO/V_2Se_2O heterostructure (see Supplemental Material [68]) and identified the most stable arrangement shown in Fig. 2(a). The corresponding band structure [Fig. 2(d)] indicates that both constituents largely preserve their intrinsic electronic features under vdW coupling. Strikingly, however, the PbO layer now exhibits pronounced momentum-dependent spin splitting [Figs. 2(d)-2(f)], in sharp contrast to its pristine spin-degenerate state [Fig. 2(b)], demonstrating that PbO is transformed into a PAM-PbO through AMPE. The induced spin splitting displays a characteristic AM signature: spin degeneracy is preserved along Γ–M, while opposite spin polarizations appear along M–X–Γ and Γ–Y–M, consistent with the underlying order of V_2Se_2O. Moreover, the real-space spin density of PAM-PbO mirrors the symmetry of the V_2Se_2O substrate, providing direct evidence that PbO inherits AM character of V_2Se_2O. To confirm this, we

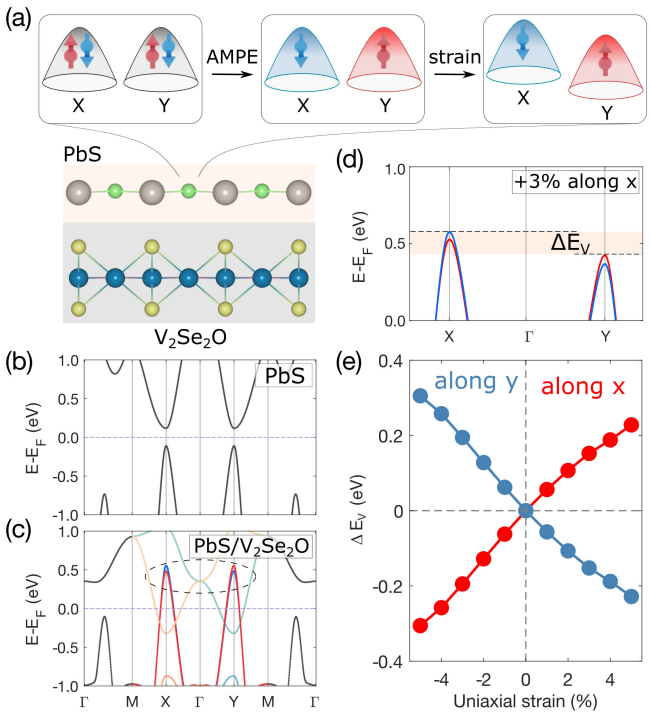

FIG. 3. **(a)** Schematic of the PbS/V_2Se_2O heterostructure illustrating the AMPE- and strain-induced spin and valley splitting in a monolayer PbS. **(b)** and **(c)** Calculated bands of the monolayer PbS and PbS/V_2Se_2O heterostructure. **(d)** Bands of the AM-proximitized monolayer PbS under 3% uniaxial tensile strain along the x axis, showing valley splitting, ΔE_V. **(e)** Strain-dependent ΔE_V. Band color codes as in Fig. 2.

further convert V_2Se_2O into a conventional AFM configuration by rearranging its spin sublattices [Fig. 2(i); see Supplemental Material [68]]. In this case, the sublattices are related by translation or inversion symmetry, eliminating the alternating spin splitting. As expected, the induced splitting in PbO disappears [Fig. 2(i)], while its spin density develops an AFM feature, indicating a conventional AFM proximity effect. This control case further illustrates the AMPE of V_2Se_2O.

To further elucidate how PbO is influenced by the AMPE of V_2Se_2O, we analyze the interfacial interaction and charge redistribution in their vdW heterostructure. The planar-averaged charge density difference $\Delta q(z)$, together with the real-space redistribution shown in Fig. 2(g), indicates charge transfer from PbO to V_2Se_2O at the interface. Because the strength of proximity effects is highly sensitive to interlayer spacing, we evaluate the evolution of the spin splitting ΔE_S as a function of the separation d between PbO and V_2Se_2O. As shown in Fig. 2(h), the induced ΔE_S decreases monotonically with increasing d, accompanied by a corresponding reduction of the spin density, confirming the short-range nature of AMPE. Taken together, these results provide unambiguous evidence for AMPE from multiple, mutually consistent perspectives.

Valleytronics— Beyond charge and spin, the valley degree of freedom provides a powerful route toward valleytronic devices and robust topological states [15, 69–72]. A common strategy to lift valley degeneracy is to apply an external magnetic field, but the typically small g-factors of semiconductors limit its effectiveness. Magnetic proximity effects offer an alternative by introducing valley asymmetry [1, 10, 11]. Valley phenomena in altermagnets have recently attracted growing attention [24, 73–75]. In particular, monolayer V_2Se_2O has been predicted to host a unique symmetry-paired spin-valley locking that links spin and valley space with real space, enabling giant piezomagnetism and large noncollinear spin currents [24].

Motivated by this, we explore whether such valley physics can be transferred into a NM material through AMPE, using a PbS/V_2Se_2O heterostructure as an example [Fig. 3(a)]. Monolayer PbS, known for its rich topological, valleytronic, and optoelectronic properties [76], exhibits spin-valley degeneracy in its pristine state [Fig. 3(b)]. When coupled to V_2Se_2O, PbS inherits the altermagnetic feature of symmetry-paired spin-valley locking through AMPE [Fig. 3(c)]. This pairing enables strain-tunable valley polarization: breaking the mirror symmetry between the X and Y valleys converts them from degenerate to polarized states. Uniaxial strain along x or y shifts their relative energies in opposite directions, producing a controllable valley splitting that grows monotonically under either compressive or tensile strain [Fig. 3(e)]. This effect is substantial even under moderate strain—for example, 3% tensile strain along x yields a 152 meV valence-band splitting [Fig. 3(d), Supplemental Material [68]], far exceeding the thermal energy at 300 K. Such a robust splitting ensures stable valley polarization and enables practical control of valley populations through mechanical or substrate engineering. These results demonstrate that AMPE provides a general route to induce spin-valley polarization in otherwise nonmagnetic materials. By combining interfacial coupling with strain engineering, one can realize electrically and mechanically tunable valley functionalities, opening new opportunities for spintronic and valleytronic applications in AM-based heterostructures.

Topological superconductivity— Proximity effects provide one of the most promising routes to realize topological superconductivity and host Majorana modes (MM), essential for fault-tolerant quantum computing [77–79]. The conventional platform——an s-wave superconductor proximitized into a semiconductor with strong spin–orbit coupling under an external magnetic field——has yielded multiple signatures of topological superconductivity [78]. However, this approach requires applied magnetic fields that compete with superconductivity. In contrast, AMPE offers a distinct advantage: it induces momentum-dependent spin splitting without net magnetization or external fields, thus preserving the superconducting gap while enabling new routes to engineer topological superconducting states [54–56].

To explore this possibility, we consider a platform composed of the well-studied vdW s-wave superconductor $NbSe_2$ placed on V_2Se_2O [Fig. 4(a)]. In this configuration, the AMPE-induced splitting from V_2Se_2O is expected to mod-

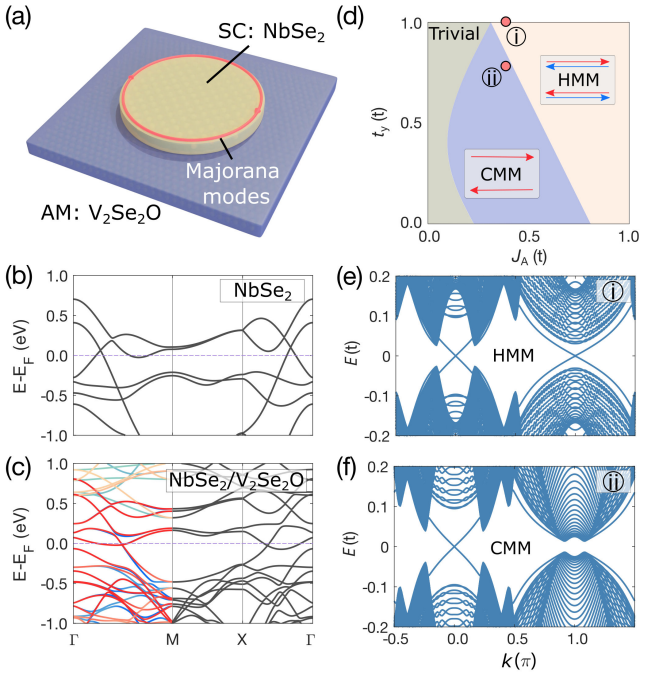

FIG. 4. **(a)** Schematic transformation of an *s*-wave superconductor $NbSe_2$ into a topological superconductor hosting edge Majorana modes (red circle) via AMPE from V_2Se_2O. **(b)** and **(c)** Bands of a $NbSe_2$ supercell and the $NbSe_2/V_2Se_2O$ heterostructure. **(d)** Topological phase diagram of the PAM-$NbSe_2$ obtained from Eq. (1). **(e)** and **(f)** Ribbon spectra of PAM-$NbSe_2$ showing helical and chiral MM (HMM and CMM). Model parameters are $t_x = 1$, $\mu = 0.6$, $\lambda_R = 0.2$, $J_A = 0.4$, $\Delta = 0.2$. $t_y = 1$ in **(e)** and $t_y = 0.8$ in **(f)**. Band color codes as in Fig. 2.

ify the pairing of $NbSe_2$ and can drive it into a topological superconductor hosting edge MM. Our first principle calculations confirm that pristine $NbSe_2$ exhibits spin-degenerate bands [Fig. 4(b)], while in the $NbSe_2/V_2Se_2O$ heterostructure these bands acquire alternating spin splitting [Fig. 4(c)], demonstrating that AMPE penetrates the superconducting layer without introducing net magnetization.

To analyze the superconducting properties, we construct a minimal effective model in the Nambu basis,

$$\begin{aligned} H_{BdG} = &\left(t_x \cos k_x + t_y \cos k_y - \mu\right)\sigma_0\tau_z \\ &+\lambda_R\left(\sin k_y \sigma_x\tau_z - \sin k_x \sigma_y\tau_z\right) \\ &+J_A\left(\cos k_x - \cos k_y\right)\sigma_z\tau_0 + \Delta\sigma_0\tau_x, \end{aligned} \tag{1}$$

where σ_i (τ_i) are Pauli matrices in spin (particle–hole) space. The model includes kinetic hopping terms $t_{x/y}$, chemical potential μ, Rashba spin-orbit coupling strength λ_R, *s*-wave pairing Δ, and an AMPE strength J_A. From gap-closing conditions and the corresponding topological invariant, we obtain the phase diagram in Fig. 4(d). For isotropic hopping ($t_x = t_y$), crystalline symmetry enforces a valley degeneracy that, with suitable J_A , yields a helical topological superconductor hosting pairs of helical MM at the edges [Fig. 4(e)]. Breaking this crystalline relation ($t_x \neq t_y$) lifts the valley degeneracy, allowing valley-selective topological transitions: one valley becomes topological while the other remains trivial. The edge spectrum then contains a single chiral MM per boundary [Fig. 4(f)]. This symmetry-controlled switch between helical and chiral MM within a single platform is a key advantage of AMPE-based designs. Because altermagnetism can be flexibly tuned by various dynamic means [29, 30, 80], AMPE enables controllable manipulation of MMs, offering unprecedented opportunities for their fusion and braiding [81–83] central to topological quantum computing. Thus, AMPE establishes a versatile and highly controllable pathway to realize topological superconductivity in vdW system.

Our proposed AMPE shifts the role of altermagnets from intrinsic or bulk mechanisms to an interfacial route. This conceptual advance significantly broadens their scope, enabling their momentum-alternating spin textures to be harnessed in otherwise NM systems. Just as ferromagnetic proximity can induce energy splittings beyond those achievable with external fields [1], AMPE offers comparable advantages while avoiding stray fields and net magnetization. This field-free distinction is especially crucial for proximity-induced topological superconductivity, where conventional Zeeman-based schemes are often limited to semiconductors with large-g factors even under magnetic textures and fringing fields [83, 84].

More broadly, the tunable spin and symmetry properties of altermagnets make AMPE a versatile platform for realizing emergent states that would otherwise demand complex materials or multiple proximity effects [1]. A natural outlook is to identify the governing factors and control knobs of AMPE strength, as well as the characteristic energy and time scales for reconfiguring altermagnetic order. Such efforts will be essential for assessing the feasibility of dynamical control over spin-dependent and topological responses [14, 85], opening new opportunities to manipulate quantum phases in both normal and superconducting states.

Acknowledgements—We thank Y. Liu for useful discussions. This work is supported by the National Natural Science Foundation of China (12474155, 12447163, and 11904250), the Zhejiang Provincial Natural Science Foundation of China (LR25A040001), the China Postdoctoral Science Foundation (2025M773440), the U.S. DOE, Office of Science BES, Award No. DE-SC0004890 (I.Ž. for AM), and the U.S. ONR under Award No. MURI N000142212764 (I.Ž. for MM). The computational resources for this research were provided by the High Performance Computing Platform at the Eastern Institute of Technology, Ningbo.

Z.Z. and R.H. contributed equally to this work.

* tzhou@eitech.edu.cn

[1] I. Žutić, A. Matos-Abiague, B. Scharf, H. Dery, and K. Belashchenko, Proximitized materials, Mater. Today **22**, 85 (2019).

[2] A. I. Buzdin, Proximity effects in superconductor-ferromagnet heterostructures, Rev. Mod. Phys. **77**, 935 (2005).

[3] J. J. Hauser, Magnetic proximity effect, Phys. Rev. **187**, 580 (1969).

[4] P. Manna and S. Yusuf, Two interface effects: Exchange bias and magnetic proximity, Phys. Rep. **535**, 61 (2014).

[5] M. Gmitra and J. Fabian, Graphene on transition-metal dichalcogenides: A platform for proximity spin-orbit physics and optospintronics, Phys. Rev. B **92**, 155403 (2015).

[6] Z. Wang, C. Tang, R. Sachs, Y. Barlas, and J. Shi, Proximity-induced ferromagnetism in graphene revealed by the anomalous Hall effect, Phys. Rev. Lett. **114**, 016603 (2015).

[7] C. Zhao, T. Norden, P. Zhang, P. Zhao, Y. Cheng, F. Sun, J. P. Parry, P. Taheri, J. Wang, Y. Yang, T. Scrace, K. Kang, S. Yang, G.-X. Miao, R. Sabirianov, G. Kioseoglou, W. Huang, A. Petrou, and H. Zeng, Enhanced valley splitting in monolayer WSe_2 due to magnetic exchange field, Nat. Nanotechnol. **12**, 757 (2017).

[8] B. Scharf, G. Xu, A. Matos-Abiague, and I. Žutić, Magnetic proximity effects in transition-metal dichalcogenides: Converting excitons, Phys. Rev. Lett. **119**, 127403 (2017).

[9] D. Zhong, K. L. Seyler, X. Linpeng, N. P. Wilson, T. Taniguchi, K. Watanabe, M. A. McGuire, K.-M. C. Fu, D. Xiao, W. Yao, and X. Xu, Layer-resolved magnetic proximity effect in van der waals heterostructures, Nat. Nanotechnol. **15**, 187 (2020).

[10] J. Choi, C. Lane, J.-X. Zhu, and S. A. Crooker, Asymmetric magnetic proximity interactions in $MoSe_2/CrBr_3$ van der waals heterostructures, Nat. Mater. **22**, 305 (2023).

[11] T. Zhou and I. Žutić, Asymmetry in the magnetic neighbourhood, Nat. Mater. **22**, 284 (2023).

[12] V. Baltz, A. Manchon, M. Tsoi, T. Moriyama, T. Ono, and Y. Tserkovnyak, Antiferromagnetic spintronics, Rev. Mod. Phys. **90**, 015005 (2018).

[13] D. Shao and E. Tsymbal, Antiferromagnetic Tunnel Junctions for Spintronics, npj Spintron. **2**, 13 (2024).

[14] I. Žutić, J. Fabian, and S. Das Sarma, Spintronics: Fundamentals and applications, Rev. Mod. Phys. **76**, 323 (2004).

[15] J. R. Schaibley, H. Yu, G. Clark, P. Rivera, J. S. Ross, K. L. Seyler, W. Yao, and X. Xu, Valleytronics in 2D materials, Nat. Rev. Mater. **1**, 16055 (2016).

[16] Z. Qiao, W. Ren, H. Chen, L. Bellaiche, Z. Zhang, A. H. MacDonald, and Q. Niu, Quantum anomalous Hall effect in graphene proximity coupled to an antiferromagnetic insulator, Phys. Rev. Lett. **112**, 116404 (2014).

[17] R. Cai, I. Žutić, and W. Han, Superconductor/ferromagnet heterostructures: A platform for superconducting spintronics and quantum computation, Adv. Quantum Technol. **6**, 2200080 (2023).

[18] L. Fu and C. L. Kane, Superconducting proximity effect and Majorana Fermions at the surface of a topological insulator, Phys. Rev. Lett. **100**, 096407 (2008).

[19] S. Hayami, Y. Yanagi, and H. Kusunose, Momentum-dependent spin splitting by collinear antiferromagnetic ordering, J. Phys. Soc. Jpn. **88**, 123702 (2019).

[20] L. Yuan, Z. Wang, J. Luo, E. Rashba, and A. Zunger, Giant momentum-dependent spin splitting in centrosymmetric low-Z antiferromagnets, Phys. Rev. B **102**, 014422 (2020).

[21] L. Šmejkal, R. González-Hernández, T. Jungwirth, and J. Sinova, Crystal time-reversal symmetry breaking and spontaneous hall effect in collinear antiferromagnets, Sci. Adv. **6**, eaaz8809 (2020).

[22] I. I. Mazin, K. Koepernik, M. D. Johannes, R. González-Hernández, and L. Šmejkal, Prediction of unconventional magnetism in doped $FeSb_2$, Proc. Natl. Acad. Sci. **118**, e2108924118 (2021).

[23] L. Yuan, Z. Wang, J. Luo, and A. Zunger, Prediction of low-Z collinear and noncollinear antiferromagnetic compounds having momentum-dependent spin splitting even without spin-orbit coupling, Phys. Rev. Mater. **5**, 014409 (2021).

[24] H. Ma, M. Hu, N. Li, J. Liu, W. Yao, J. Jia, and J. Liu, Multifunctional antiferromagnetic materials with giant piezomagnetism and noncollinear spin current, Nat. Commun. **12**, 2846 (2021).

[25] Y.-P. Zhu, X. Chen, X.-R. Liu, Y. Liu, P. Liu, H. Zha, G. Qu, C. Hong, J. Li, Z. Jiang, X.-M. Ma, Y.-J. Hao, M.-Y. Zhu, W. Liu, M. Zeng, S. Jayaram, M. Lenger, J. Ding, S. Mo, K. Tanaka, M. Arita, Z. Liu, M. Ye, D. Shen, J. Wrachtrup, Y. Huang, R.-H. He, S. Qiao, Q. Liu, and C. Liu, Observation of plaid-like spin splitting in a noncoplanar antiferromagnet, Nature **626**, 523 (2024).

[26] Q. Liu, X. Dai, and S. Blügel, Different facets of unconventional magnetism, Nat. Phys. **21**, 329 (2025).

[27] L. Šmejkal, J. Sinova, and T. Jungwirth, Beyond conventional ferromagnetism and antiferromagnetism: A phase with nonrelativistic spin and crystal rotation symmetry, Phys. Rev. X **12**, 031042 (2022).

[28] L. Šmejkal, J. Sinova, and T. Jungwirth, Emerging research landscape of altermagnetism, Phys. Rev. X **12**, 040501 (2022).

[29] L. Bai, W. Feng, S. Liu, L. Šmejkal, Y. Mokrousov, and Y. Yao, Altermagnetism: Exploring new frontiers in magnetism and spintronics, Adv. Funct. Mater. **34**, 2409327 (2024).

[30] C. Song, H. Bai, Z. Zhou, L. Han, H. Reichlova, J. H. Dil, J. Liu, X. Chen, and F. Pan, Altermagnets as a new class of functional materials, Nat. Rev. Mater. **10**, 473 (2025).

[31] J. Krempaskỳ, L. Šmejkal, S. D'Souza, M. Hajlaoui, G. Springholz, K. Uhlířová, F. Alarab, P. Constantinou, V. Strocov, D. Usanov, W. Pudelko, R. Gonzàlez-Hernàndez, A. Birk Hellenes, Z. Jansa, H. Reichlovà, Z. Šobáň, R. Gonzalez Betancourt, P. Wadley, J. Sinova, D. Kriegner, J. Minár, J. Dil, and T. Jungwirth, Altermagnetic lifting of Kramers spin degeneracy, Nature **626**, 517 (2024).

[32] Z. Zhou, X. Cheng, M. Hu, R. Chu, H. Bai, L. Han, J. Liu, F. Pan, and C. Song, Manipulation of the altermagnetic order in CrSb via crystal symmetry, Nature **638**, 645 (2025).

[33] F. Zhang, X. Cheng, Z. Yin, C. Liu, L. Deng, Y. Qiao, Z. Shi, S. Zhang, J. Lin, Z. Liu, M. Ye, Y. Huang, X. Meng, C. Zhang, T. Okuda, K. Shimada, S. Cui, Y. Zhao, G.-H. Cao, S. Qiao, J. Liu, and C. Chen, Crystal-symmetry-paired spin-valley locking in a layered room-temperature metallic altermagnet candidate, Nat. Phys. **21**, 760 (2025).

[34] B. Jiang, M. Hu, J. Bai, Z. Song, C. Mu, G. Qu, W. Li, W. Zhu, H. Pi, Z. Wei, Y.-J. Sun, Y. Huang, X. Zheng, Y. Peng, L. He, S. Li, J. Luo, Z. Li, G. Chen, H. Li, H. Weng, and T. Qian, A metallic room-temperature d-wave altermagnet, Nat. Phys. **21**, 754 (2025).

[35] S. Sheoran and P. Dev, Spontaneous anomalous Hall effect in two-dimensional altermagnets, Phys. Rev. B **111**, 184407 (2025).

[36] R. Chen, Z.-M. Wang, K. Wu, H.-P. Sun, B. Zhou, R. Wang, and D.-H. Xu, Probing k-space alternating spin polarization via the anomalous Hall effect, Phys. Rev. Lett. **135**, 096602 (2025).

[37] T. Jungwirth, J. Sinova, P. Wadley, D. Kriegner, H. Reichlova, F. Krizek, H. Ohno, and L. Smejkal, Altermagnetic spintronics, arXiv:2508.09748 (2025).

[38] D.-F. Shao, S.-H. Zhang, M. Li, C.-B. Eom, and E. Y. Tsymbal, Spin-neutral currents for spintronics, Nat. Commun. **12**, 7061 (2021).

[39] R. Takagi, R. Hirakida, Y. Settai, R. Oiwa, H. Takagi, A. Ki-

taori, K. Yamauchi, H. Inoue, J.-i. Yamaura, D. Nishio-Hamane, S. Itoh, S. Aji, H. Saito, T. Nakajima, T. Nomoto, R. Arita, and S. Seki, Spontaneous Hall effect induced by collinear antiferromagnetic order at room temperature, Nat. Mater. **24**, 63 (2025).
[40] X. Chen, Y. Liu, P. Liu, Y. Yu, J. Ren, J. Li, A. Zhang, and Q. Liu, Unconventional magnons in collinear magnets dictated by spin space groups, Nature **640**, 349 (2025).
[41] X. Duan, J. Zhang, Z. Zhu, Y. Liu, Z. Zhang, I. Žutić, and T. Zhou, Antiferroelectric altermagnets: Antiferroelectricity alters magnets, Phys. Rev. Lett. **134**, 106801 (2025).
[42] Z. Zhu, X. Duan, J. Zhang, B. Hao, I. Žutić, and T. Zhou, Two-dimensional ferroelectric altermagnets: From model to material realization, Nano Lett. **25**, 9456 (2025).
[43] Z. Zhu, Y. Liu, X. Duan, J. Zhang, B. Hao, S.-H. Wei, I. Žutić, and T. Zhou, Emergent multiferroic altermagnets and spin control via noncollinear molecular polarization, Sci. China Phys. Mech. Astron. (2025).
[44] M. Gu, Y. Liu, H. Zhu, K. Yananose, X. Chen, Y. Hu, A. Stroppa, and Q. Liu, Ferroelectric switchable altermagnetism, Phys. Rev. Lett. **134**, 106802 (2025).
[45] W. Sun, C. Yang, W. Wang, Y. Liu, X. Wang, S. Huang, and Z. Cheng, Proposing altermagnetic-ferroelectric type-III multiferroics with robust magnetoelectric coupling, Adv. Mater. **37**, 2502575 (2025).
[46] R. Cao, R. Dong, R. Fei, and Y. Yao, Designing spin-driven multiferroics in altermagnets, arXiv:2412.20347 (2024).
[47] W.-T. Guo, J. Xu, Y. Yang, H. Wang, and H. Zhang, Altermagnetic type-II multiferroics with Néel-order-locked electric polarization, arXiv:2505.01964 (2025).
[48] H.-Y. Ma and J.-F. Jia, Altermagnetic topological insulator and the selection rules, Phys. Rev. B **110**, 064426 (2024).
[49] P.-J. Guo, Z.-X. Liu, and Z.-Y. Lu, Quantum anomalous Hall effect in collinear antiferromagnetism, npj Comput. Mater. **9**, 70 (2023).
[50] P. Feng, C.-Y. Tan, M. Gao, X.-W. Yan, Z.-X. Liu, P.-J. Guo, F. Ma, and Z.-Y. Lu, Type-II quantum spin Hall insulator, arXiv:2503.13397 (2025).
[51] R.-W. Zhang, C. Cui, Y. Wang, J. Duan, Z.-M. Yu, and Y. Yao, Quantized spin-Hall conductivity in altermagnet Fe_2Te_2O with mirror-spin coupling, arXiv:2503.10681 (2025).
[52] J. Nag, B. Das, S. Bhowal, Y. Nishioka, B. Bandyopadhyay, S. Sarker, S. Kumar, K. Kuroda, V. Gopalan, A. Kimura, K. G. Suresh, and A. Alam, GdAlSi: An antiferromagnetic topological Weyl semimetal with nonrelativistic spin splitting, Phys. Rev. B **110**, 224436 (2024).
[53] B. Brekke, A. Brataas, and A. Sudbø, Two-dimensional altermagnets: Superconductivity in a minimal microscopic model, Phys. Rev. B **108**, 224421 (2023).
[54] Y.-X. Li and C.-C. Liu, Majorana corner modes and tunable patterns in an altermagnet heterostructure, Phys. Rev. B **108**, 205410 (2023).
[55] D. Zhu, Z.-Y. Zhuang, Z. Wu, and Z. Yan, Topological superconductivity in two-dimensional altermagnetic metals, Phys. Rev. B **108**, 184505 (2023).
[56] S. A. A. Ghorashi, T. L. Hughes, and J. Cano, Altermagnetic routes to Majorana modes in zero net magnetization, Phys. Rev. Lett. **133**, 106601 (2024).
[57] J. A. Ouassou, A. Brataas, and J. Linder, dc Josephson effect in altermagnets, Phys. Rev. Lett. **131**, 076003 (2023).
[58] P. Lazić, K. D. Belashchenko, and I. Žutić, Effective gating and tunable magnetic proximity effects in two-dimensional heterostructures, Phys. Rev. B **93**, 241401 (2016).
[59] J. Xu, S. Singh, J. Katoch, G. Wu, T. Zhu, I. Žutić, and R. K. Kawakami, Spin inversion in graphene spin valves by gate-tunable magnetic proximity effect at one-dimensional contacts, Nat. Commun. **9**, 2869 (2018).
[60] P. E. Faria Junior, T. Naimer, K. M. McCreary, B. T. Jonker, J. J. Finley, S. A. Crooker, J. Fabian, and A. V. Stier, Proximity-enhanced valley Zeeman splitting at the WS_2/graphene interface, 2D Mater. **10**, 034002 (2023).
[61] K. Zollner, P. E. Faria Junior, and J. Fabian, Strong manipulation of the valley splitting upon twisting and gating in $MoSe_2/CrI_3$ and WSe_2/CrI_3 van der waals heterostructures, Phys. Rev. B **107**, 035112 (2023).
[62] K. Huang, E. Schwartz, D.-F. Shao, A. A. Kovalev, and E. Y. Tsymbal, Magnetic antiskyrmions in two-dimensional van der Waals magnets engineered by layer stacking, Phys. Rev. B **109**, 024426 (2024).
[63] X. Xi, Z. Wang, W. Zhao, J.-H. Park, K. T. Law, H. Berger, L. Forró, J. Shan, and K. F. Mak, Ising pairing in superconducting $NbSe_2$ atomic layers, Nat. Phys. **12**, 139 (2016).
[64] D. Wickramaratne, S. Khmelevskyi, D. F. Agterberg, and I. I. Mazin, Ising superconductivity and magnetism in $NbSe_2$, Phys. Rev. X **10**, 041003 (2020).
[65] H. Lin, J. Si, X. Zhu, K. Cai, H. Li, L. Kong, X. Yu, and H.-H. Wen, Structure and physical properties of $CsV_2Se_{2-x}O$ and V_2Se_2O, Phys. Rev. B **98**, 075132 (2018).
[66] S. Barraza-Lopez, B. M. Fregoso, J. W. Villanova, S. S. Parkin, and K. Chang, Colloquium: Physical properties of group-IV monochalcogenide monolayers, Rev. Mod. Phys. **93**, 011001 (2021).
[67] P. Kumar, J. Liu, P. Ranjan, Y. Hu, S. S. Yamijala, S. K. Pati, J. Irudayaraj, and G. J. Cheng, Alpha lead oxide (α-PbO): A new 2D material with visible light sensitivity, Small **14**, 1703346 (2018).
[68] See Supplemental Material for the expanded discussion of the first-principles calculation methods, different stacking configurations, band structures under strain.
[69] D. Xiao, W. Yao, and Q. Niu, Valley-contrasting physics in graphene: Magnetic moment and topological transport, Phys. Rev. Lett. **99**, 236809 (2007).
[70] T. Zhou, S. Cheng, M. Schleenvoigt, P. Schüffelgen, H. Jiang, Z. Yang, and I. Žutić, Quantum spin-valley Hall kink states: From concept to materials design, Phys. Rev. Lett. **127**, 116402 (2021).
[71] T. Zhou, J. Zhang, B. Zhao, H. Zhang, and Z. Yang, Quantum spin-quantum anomalous Hall insulators and topological transitions in functionalized Sb(111) monolayers, Nano Lett. **15**, 5149 (2015).
[72] T. Zhou, J. Zhang, H. Jiang, I. Žutić, and Z. Yang, Giant spin-valley polarization and multiple Hall effect in functionalized bismuth monolayers, npj Quantum Mater. **3**, 39 (2018).
[73] R.-W. Zhang, C. Cui, R. Li, J. Duan, L. Li, Z.-M. Yu, and Y. Yao, Predictable gate-field control of spin in altermagnets with spin-layer coupling, Phys. Rev. Lett. **133**, 056401 (2024).
[74] Y.-Q. Li, Y.-K. Zhang, X.-L. Lu, Y.-P. Shao, Z.-Q. Bao, J.-D. Zheng, W.-Y. Tong, and C.-G. Duan, Ferrovalley physics in stacked bilayer altermagnetic systems, Nano Lett. **25**, 6032 (2025).
[75] S.-D. Guo, Y. Liu, J. Yu, and C.-C. Liu, Valley polarization in twisted altermagnetism, Phys. Rev. B **110**, L220402 (2024).
[76] W. Wan, Y. Yao, L. Sun, C.-C. Liu, and F. Zhang, Topological, valleytronic, and optical properties of monolayer PbS, Adv. Mater. **29**, 1604788 (2017).
[77] K. Flensberg, F. von Oppen, and A. Stern, Engineered platforms for topological superconductivity and Majorana zero modes, Nat. Rev. Mater. **6**, 944 (2021).

[78] S. D. Sarma, M. Freedman, and C. Nayak, Majorana zero modes and topological quantum computation, npj Quantum Inf. **1**, 15001 (2015).

[79] U. Güngördü and A. A. Kovalev, Majorana bound states with chiral magnetic textures, J. Appl. Phys. **132**, 041101 (2022).

[80] Y. Chen, X. Liu, H.-Z. Lu, and X. C. Xie, Electrical switching of altermagnetism, Phys. Rev. Lett. **135**, 016701 (2025).

[81] T. Zhou, M. C. Dartiailh, K. Sardashti, J. E. Han, A. Matos-Abiague, J. Shabani, and I. Žutić, Fusion of Majorana bound states with mini-gate control in two-dimensional systems, Nat. Commun. **13**, 1738 (2022).

[82] T. Zhou, M. C. Dartiailh, W. Mayer, J. E. Han, A. Matos-Abiague, J. Shabani, and I. Žutić, Phase control of Majorana bound states in a topological X junction, Phys. Rev. Lett. **124**, 137001 (2020).

[83] G. L. Fatin, A. Matos-Abiague, B. Scharf, and I. Žutić, Wireless Majorana bound states: From magnetic tunability to braiding, Phys. Rev. Lett. **117**, 077002 (2016).

[84] T. Zhou, N. Mohanta, J. E. Han, A. Matos-Abiague, and I. Žutić, Tunable magnetic textures in spin valves: From spintronics to Majorana bound states, Phys. Rev. B **99**, 134505 (2019).

[85] M. Amundsen, J. Linder, J. W. A. Robinson, I. Žutić, and N. Banerjee, Colloquium: Spin-orbit effects in superconducting hybrid structures, Rev. Mod. Phys. **96**, 021003 (2024).